# SIMULATION OF HELICOPTER SEE-SAW ROTOR MOTION

Janusz Narkiewicz, Wiesław Łucjanek
Warsaw University of Technology, Warsaw, Poland

Abstract

The model developed to simulate the motion of helicopter see-saw rotor consists of two elastic blades attached to the deformable shaft with pitch and skew flap hinges. The deformable blades can bend in two perpendicular directions and twist around the straight elastic axis. Nonlinear steady two-dimensional airfoil data are used for aerodynamic loads calculations. The unsteady flow effects are described by dynamic inflow model.

The equations of motion are generated from Hamilton's principle in semi-automatic way with most of algebraic manipulations done by computer. The blade deflections are discretized by free vibration modes calculated for rotating blades.

The model can be incorporated into computer software for numerical integration and stability analysis.

The sample results concern investigation of blade steady motion and dynamic inflow modeling on rotor behaviour.

## 1. INTRODUCTION.

Although attempts are made to replace tail rotors by other devices [1],[2], tail rotors still remain the most often used anti-torque and yaw control systems. Tail rotors have often two blades of see-saw type. Helicopter two-bladed main rotors are also design of this type.

There are not many references concerning two blade rotors [3-7]. although some aeroelastic stability problems [8], [9] are typical for see-saw rotors (egs. blade weaving).

The model developed in this paper is to be used for investigation of see-saw rotor aeroelastic behavior. The derivation of equations of motion is done in semi-automatic way. The computer program based on this model is incorporated into the software developed for rotor motion simulation and stability investigation [10].

The influence of dynamic inflow and blade steady state position on rotor stability is investigated in this paper.

## 2. ROTOR MODEL.

The rotor on helicopter in steady flight or on wind-tunnel stand is considered. External flow velocity components can vary in time so the influence of gusts and wind can be analyzed.

The rotor model (Fig.1) consists of two blades attached with stiff elements AO, OB to the flap hinge placed on the shaft axis. The flap hinge axis is skewed by the angle $\delta$ from the axis

perpendicular to the plane of the elements A-B. The precone angles of elements AO and OB and the flap hinge spring can be included into analysis. The shaft and drive system torsional flexibility is modeled as torsional spring placed near the hub.

The rotor shaft angular velocity $\Omega$ is constant.

For pitch control the blades have feathering hinges axes of which are swept by the angle $\tau$ in the plane of rotation (positive $\tau$ is opposite to the azimuth angle $\psi$). The blade control system flexibility is included into boundary conditions for blades torsional deflections. The kinematic pitch-flap coupling different from flap hinge axis skewing effect is included into analysis.

Each blade has straight elastic axis parallel to feathering axis. The blades are twisted geometrically around elastic axis. The blade can bend in two perpendicular directions and twist around elastic axis.

## 3. EQUATIONS OF MOTION

### 3.1. General remarks.

The equations of motion have been obtained with the method developed in [11]. The derivation of equations of motion is based on the Hamilton's principle in the form:

$$\int_{t_1}^{t_2} [\delta(U-T)-\delta W]dt=0. \qquad (1)$$

The blade motion is described by:

1. "Rigid degrees of freedom":
   - shaft torsion angle $\vartheta$,
   - flap angle $\beta$.
2. "Elastic degrees of freedom"; for each blade (k=1,2):
   - in-plane bending deflection $v_k$,
   - out-of-plane bending deflection $w_k$,
   - torsion of the blade $\Phi_k$.

The vector of generalized coordinates for rotor motion is:

$$q = [\ q_i\ ]^T = [v_1, w_1, \Phi_1, v_2, w_2, \Phi_2, \beta, \vartheta]^T, \quad (i=1,2,.....,N_d). \qquad (2)$$

The deflections were discretized by blades free vibration modes. The same numbers of modes were assumed for each blade.

The variations of T and U in (2) are calculated in terms of the generalized coordinates and velocities variations and after using identity $\delta d=d\delta$ and integrating by parts, the expressions which contain the velocity variations are eliminated.

Two kinds of equations of motion are obtained:
- for "rigid degrees of freedom" $(i=1,2,....N_r)$:

$$\frac{d}{dt}\left(\frac{\partial T}{\partial \dot{q}_i}\right) - \frac{\partial T}{\partial q_i} + \frac{\partial U}{\partial q_i} = Q_n, \qquad (3a)$$

- for elastic degrees of freedom ($i=1,2,\ldots N_e$):

$$\int_R \left[ \frac{d}{dt}\left( \frac{\partial T}{\partial \dot{q}_i} \right) - \frac{\partial T}{\partial q_i} + \frac{\partial U}{\partial q_i} \right] \eta_i \, dR + \int_R \left[ \frac{d}{dt}\left( \frac{\partial T}{\partial \dot{q}_i} \right) - \frac{\partial T}{\partial q_i} + \frac{\partial U}{\partial q_i} \right] \eta_i' \, dR$$

$$+ \int_R \left[ \frac{\partial U}{\partial \dot{q}_i''} \right] \eta_i'' \, dR = \int_R Q_n \eta_i \, dR. \qquad (3b)$$

The integration in (2) extends along both blades.

In these equations:
- inertia loads result from derivatives of kinetic energy,
- stiffness loads come from potential energy,
- nonconservative loads arise from aerodynamic and damping forces.

3.2. Inertia loads.

The kinetic energy T can be defined in the form:

$$T = \frac{1}{2} \int_R \int_{A_s} \rho_b \dot{\mathbf{x}}^2 dA_s \, dR. \qquad (4)$$

In [4] the vector $\mathbf{x}$ describing the blade point in the inertial frame of coordinates is obtained as:

$$\mathbf{x} = \mathbb{D}(\psi)\mathbf{r}_o = \mathbb{D}(\psi)(\mathbf{r}+\mathbb{A}\mathbf{x}_1+\mathbb{A}\mathbf{s}), \qquad (5)$$

where: $\mathbb{A} = \mathbb{A}_R(\delta)\mathbb{A}_B(\vartheta)\mathbb{B}(\beta)\mathbb{C}_1(\delta)\mathbb{C}_2(\tau)\mathbb{G}(\theta_o)$, (5a)

$$\mathbf{r}_o = \mathbf{r}+\mathbb{A}(\mathbf{x}_1+\mathbf{s}), \qquad (5b)$$

$$\mathbf{r} = \mathbb{A}_R(\delta)\mathbb{A}_B(\vartheta)\mathbb{B}(\beta)\mathbb{C}_1(\delta)[\mathbf{e}_o+\mathbb{C}_2(\tau)\mathbb{G}(\theta_o)\mathbf{f}_o], \qquad (5c)$$

$$\mathbf{x}_1 + \mathbf{s} = \mathbf{x}_2+\mathbf{v}+\mathbb{T}\boldsymbol{\xi} = \mathbf{x} + \Sigma\mathbf{s}_i, \quad (i=1,2,3). \qquad (5d)$$

Matrices and vectors of (5) are given in Appendix 1.

After inserting (5) into (4) and then into (3) the inertia loads (I.L.) are obtained in the matrix form:

$$\text{I.L.} = \mathbb{B}(\mathbf{q})\ddot{\mathbf{q}}+2\mathbb{C}(\mathbf{q})\dot{\mathbf{q}}+\dot{\mathbf{q}}^T\mathbb{D}_n(\dot{\mathbf{q}})\mathbf{q}+\mathbf{f}(\mathbf{q}). \qquad (6)$$

The matrices $\mathbb{B}$, $\mathbb{C}$, $\mathbb{D}_n$ and vector $\mathbf{f}$ are given in Appendix 2.

3.3. Stiffness loads.

Stiffness loads consist of shaft and flap hinge springs deformations moments and forces due to blade deflections.

The rotor shaft and flap hinge spring deformations can be arbitrary functions of the angles $\vartheta$ and $\beta$ respectively.

Blade deformation forces and moments are derived from model given in [11]. It is assumed that deformations are small, and there is no section warping. Blade cross sections have the symmetry of elastic properties about the chord.

The general expression for beam elastic strain energy, after applying the Hooke's law, has the form:

$$U = \frac{1}{2}\int_{R}\int_{A_s}[E\varepsilon_{11}^2+2G(\varepsilon_{12}^2+\varepsilon_{13}^2)]dA_s dR. \tag{7}$$

After expressing the strain tensor components as the functions of generalized coordinates, eliminating blade longitudinal extensions, allowing for first terms of v, w and $\Phi$ and linearizing sin and cos about $\Phi$, the expressions for strains were put into (7).

The stiffness loads (S.L.) in the equations of motion due to blade deflections can be put in the form:

$$S.L = \mathbb{Q}\mathbf{q} + \mathbf{h}. \tag{8}$$

The elements of matrix $\mathbb{Q}$ and vector $\mathbf{h}$ are given in [11].

This model has been chosen here for its simplicity but any other even more sophisticated elastic load model can be easily incorporated into the equations of motion.

3.4. Aerodynamic loads.

Aerodynamic loads calculations are based on the strip theory. In each blade cross section the 2D flow is assumed. The aerodynamic loads acting in section aerodynamic center A.C. consist of:

- drag: $dD=\frac{1}{2}\rho c(x)V^2C_D(\alpha)dx,$ (9a)

- lift: $dL=\frac{1}{2}\rho c(x)V^2C_L(\alpha)dx,$ (9b)

- moment: $dM=\frac{1}{2}\rho c^2(x)V^2C_M(\alpha)dx.$ (9c)

The airfoil aerodynamic coefficients are calculated from 2D steady, nonlinear characteristics for instant angles of attack $\alpha$.

The section flow velocity $\mathbf{V}$ results from:
- flight (or wind-tunnel) velocity $\mathbf{V}_L$,
- rotor motion relative to the helicopter fuselage $\dot{\mathbf{x}}$,
- induced velocity $\mathbf{v}_i$.

and can be expressed as:

$$\mathbf{V}=(\mathbb{AT})^{-1}\left[\mathbf{V}_L+\mathbf{v}_i+\dot{\mathbf{x}}\right]. \tag{10}$$

The dynamic inflow model used for induced velocity calculations allows to account into analysis the effects of unsteady flow. The induced velocity vector consists of only one component perpendicular to the plane of rotation.

Total induced velocity is a sum of constant part obtained from momentum theory and perturbations due to dynamic inflow:

$$\lambda=\lambda_o+\lambda_i. \tag{11}$$

Perturbations of induced velocity vector are calculated using coefficients [12].

The aerodynamic loads in the blade section can be expressed as force and moment vectors:

$$\mathbf{f}_A=[f_\xi, f_\eta, f_\zeta]^T, \qquad \mathbf{m}_A=[m_\xi, m_\eta, m_\zeta]^T, \tag{12}$$

$$f_\xi=0, \qquad m_\xi=-dM+\eta_A f_\zeta,$$
$$f_\eta= dD\cos(\alpha)-dL\sin(\alpha), \qquad m_\eta=0,$$
$$f_\zeta= dD\sin(\alpha)+dL\cos(\alpha), \qquad m_\zeta=0.$$

The vector of rotor aerodynamic loads in the equations of motion:

$$Q_A=Q_A(t,q,\dot{q})=[Q_{Ai}]^T, \qquad (i=1,2,..,N_d), \tag{13}$$

can be obtained from (12) by successive transformations.

The loads (12) are transformed to the section coordinates system:

$$\mathbf{f}_{A2}=\mathbb{T}\mathbf{f}_A, \qquad \mathbf{m}_{A2}=\mathbb{T}\mathbf{m}_A \tag{14}$$

and to the equations of motion the components of aerodynamic loading are taken from (14) for:

- in-plane bending: $$Q_{Ai}=\int_R \eta_1 f_{A2Y}\,dR, \quad (i=N_A+1,\ldots,N_v), \tag{15a}$$

- out-of-plane bending: $$Q_{Ai}=\int_R \eta_1 f_{A2Z}\,dR, \quad (i=N_A+N_v+1,..,N_A+N_v+N_w), \tag{15b}$$

- for torsion: $$Q_{Ai}=\int_R \eta_1 m_{A2X}\,dR, \quad (i=N_A+N_v+N_w+1,..,N_A+2*N_c), \tag{15c}$$

$N_A=1$ for I blade,
$N_A=N_c$ for II blade.

The next steps of aerodynamic loads calculation are: transformation to the feathering axis at the root of the blade, calculation of the total blade loads in the feathering coordinate system:

$$\mathbf{F}_{A1} = \int_R \mathbf{f}_{A1}\,dR, \qquad \mathbf{M}_{A1} = \int_R \mathbf{m}_{A1}\,dR. \tag{16}$$

The aerodynamic loads in flap hinge coordinate system are obtained as:

$$\mathbf{F}_{AB}=\mathbb{B}(\beta)\mathbb{C}_1(\delta)\mathbb{C}_2(\tau)\mathbb{G}(\theta_o)\mathbf{F}_{A1}, \tag{17}$$
$$\mathbf{M}_{AB}=\mathbb{B}(\beta)\mathbb{C}_1(\delta)\left[\mathbb{C}_2(\tau)\mathbb{G}(\theta_o)\mathbf{M}_{A1}+e\times\mathbb{C}_2(\tau)\mathbb{G}(\theta_o)\mathbf{F}_{A1}\right].$$

From (17) the moment component along flap hinge axis is taken into the rotor flap equation:

$$Q_{Ai}=M_{ABY}, \qquad (i=2*N_c+1). \tag{18}$$

Next, the aerodynamic loads in the shaft system coordinates are obtained:

$$\mathbf{F}_{AR}=\mathbb{A}_B(\vartheta)\mathbf{F}_{AB}, \qquad \mathbf{M}_{AR}=\mathbb{A}_B(\vartheta)\mathbf{M}_{AB} \tag{19}$$

and the component along the rotor shaft is taken into the equation of shaft deformation:

$$Q_{Ai}=M_{ABZ}, \qquad (i=2*N_e+2). \tag{20}$$

The rotor aerodynamic loads for dynamic inflow model are calculated as:

$$\mathbf{F}_{AS}=\mathbb{A}_R(\delta)\mathbf{F}_{AR}, \qquad \mathbf{M}_{AS}=\mathbb{A}_R(\delta)\mathbf{M}_{AR}. \tag{21}$$

3.5. Damping moments

The damping forces can be described as a vector:

$$\mathbf{F}_D=\mathbf{F}_D(q_i,\dot{q}_i)=[F_{Di}]^T, \qquad (i=1,2,..,N_d). \tag{22}$$

Moments for shaft torsion and flap hinge damping can be arbitrary function of shaft torsion and flap angles and angular velocities:

$$F_{Di}=F_{Di}(q_i,\ \dot{q}_i), \qquad (i=N_e+1,..,N_e+2). \tag{23}$$

For blades deflections the viscous damping loads are modeled in the form:

$$F_{Di}=\dot{q}_i\int_R \eta_i\gamma_i\,dR, \qquad (i=1,2,\ldots,N_d). \tag{24}$$

3.6. Final form of equations of motion

After collecting together the expressions: (6), (8), (13), (22) the equations of motion are put in the form:

$$\mathbb{B}(q)\ddot{q}=-2\mathbb{C}(q)\dot{q}-\dot{q}^T\mathbb{D}_n(q)\dot{q}-\mathbf{f}(q)-\mathbb{Q}q-\mathbf{h}-\mathbf{F}_D(q,\dot{q})+\mathbf{Q}_A(t,q,\dot{q}). \tag{25}$$

Most of algebraic manipulations needed for generation of these equations are performed by computer. The derivatives of transformation matrices and translation vectors were calculated analytically to avoid numerical difficulties. The blade generalized masses and stiffnesses are obtained from the separate computer program before solving these equations, so the inertial and structural operators need not be integrated along the blade span during the computation of equation right hand sides.

The equations are adopted to computer software allowing for numerical integration, linearization and stability analysis.

## 4. SAMPLE RESULTS

The model was applied for investigation of influence of inflow model and steady motion parameters on see-saw rotor stability motion. This problem has not been investigated so far.

The dynamic inflow contribution to the rotor motion was analyzed for two cases:
A. full model with dynamic inflow coefficients.
B. no inflow perturbation, $\lambda_i = 0$.

The rotor motion for rigid blade is shown in Fig 2. The influence of inflow modeling is evident.

The influence of inflow on eigenvalues of sample elastic blade deformations is illustrated in Table I. Dynamic inflow included into model changes mainly in-plane and pitch deformations and has less influence on out-of-plane stability.

## 5. CONCLUSIONS

The model was developed for simulating a see-saw rotor motion for helicopter in steady flight.

The method which was applied for derivation of equations of motion enables easy modifications, extensions and incorporation of new model elements.

The model was used to investigation of inflow modeling on rotor motion.

Acknowledgements.
Authors would like to express their gratitude to Mr. Tomasz Bartler for using his graphic software in preparing this paper.

## BIBLIOGRAPHY

1. Logan A.H., Morger K.M., Sampatacos E.P., "Design, development and testing of the no tail rotor (NOTAR) demonstrator", **Proceedings of IX ERF-1983**, Paper No.067.
2. Vuillet A., "Operational advantages and power efficiency of the Fenestron as compared to a conventional tail rotor", **Vertiflite**, Vol.35, No.5, 1989.
3. Payne P.R., "Helicopter dynamics and aerodynamics", Sir Isaac Pitman & Sons, Ltd, London, 1959.
4. Johnson W., "Helicopter theory", Princeton University Press, Princeton, New Jersey, 1980.
5. Shamie J., Friedmann P., "Aeroelastic stability of complete rotors with application to a teetering rotor in forward flight", **Journal of Sound and Vibration** (1977), **53**(4), 559-584.
6. Kawakami N., "Dynamic of an elastic seesaw rotor", **Journal of Aircraft**, Vol.14, No.3, March 1977.

7. Kaza K.R.V., Janetzke D.C., Sullivan T.L., "Evaluation of MOSTAS computer code for predicting dynamic loads in two-bladed wind turbines", **AIAA Paper.** No.79-0733.

8. Zvolanek I., "Stability of an unsymmetric rotor on an unsymmetric support", **Journal of the American Helicopter Society**, Vol.34, No.4, January 1979.

9. Chen S.Y., "Stability of two-bladed aeroelastic rotors on flexible supports", **Journal of the American Helicopter Society**, Vol.38, No.1, January 1983.

10. Narkiewicz J., Łucjanek W., "General model of isolated helicopter blade for stability investigation", **Proceedings of XVI ERF-1990**, Paper No. III.8.2.

11. Houbolt J.C., Brooks G.W., "Differential equations of motion for combined flapwise bending, chordwise bending and torsion of twisted nonuniform rotor blades", **NACA Rep.** 1346, 1957.

12. Pitt D.M, Peters D.A., "Theoretical prediction of dynamic inflow derivatives", **Vertica**, Vol.5, No.1, 1981.

NOTATION

$A_s$ - blade section area,
$\mathbb{B}(q)$ - inertia matrix,
$c(x)$ - blade section chord,
$\mathbb{C}(q)$ - Coriolis loading matrix,
$C_{()}$ - aerodynamic coefficients: D-drag, L-lift, M-moment,
$\mathbb{D}_n(q)$ - gyroscopic loads matrices $(n=1,\ldots,N_e)$,
$\mathbf{e}$ - vector of feathering hinge location, $\mathbf{e} = [e_x, e_y, e_z]^T$,
$E$ - Young modulus,
$\mathbf{f}_o$ - vector of elastic axis location, $\mathbf{f}_o = [f_x, f_y, f_z]^T$,
$\mathbf{f}(q)$ - vector in the expressions of inertia loads,
$\mathbf{f}_{A()}$ - section aerodynamic force,
$\mathbf{F}_{A()}$ - rotor aerodynamic force,
$\mathbf{F}_D$ - vector of damping moments,
$G$ - Kirkhoff modulus,
$K_p$ - control system stiffness,
$K_W$ - shaft and drive system stiffness,
$\mathbf{m}_{A()}$ - section aerodynamic moment,
$\mathbf{M}_{A()}$ - rotor aerodynamic moment,
$N_c$ - number of blade deflections, $N_c = N_v + N_w + N_\Phi$,
$N_d$ - number of generalized coordinates, $N_d = 2*N_c + N_r$,
$N_r$ - number of "rigid degrees of freedom", $N_r = 2$,
$N_V$ - number of in-plane bending deflection modes for one blade,
$N_W$ - number of out-of-plane bending deflection modes for one blade,

$N_\Phi$ - number of torsion deflection modes for one blade,

$\mathbf{q}$ - vector of generalized coordinates,

$Q_n$ - nonconservative forces in Hamilton's equations of motion,

$\mathbf{Q}_A$ - vector of aerodynamic loading in equations of motion,

$R$ - rotor radius,

$t$ - time,

$T$ - kinetic energy, $T = T(t, \mathbf{q}, \dot{\mathbf{q}}, \mathbf{q}', \dot{\mathbf{q}}')$,

$U$ - potential energy, $U = U(\mathbf{q}, \mathbf{q}', \mathbf{q}'')$,

$\mathbf{v}$ - blade translation vector due to deflections, $\mathbf{v}=[0, v, w]^T$,

$\mathbf{v}_i$ - induced velocity,

$v_k$ - in-plane bending deflections of the k-th blade,

$V$ - flow velocity in the blade section, $V_p^2=V_{Ly}^2+V_{Lz}^2$,

$\mathbf{V}$ - blade section flow velocity vector,

$V_L$ - flight (or wind-tunnel) velocity,

$w_k$ - out-of-plane bending deflection of the k-th blade,

$W$ - work of nonconservative forces, $W = W(t, \mathbf{q}, \dot{\mathbf{q}}, \mathbf{q}', \dot{\mathbf{q}}')$,

$\beta$ - angle of rotation in flap hinge,

$\beta_p$ - blade precone angle,

$\gamma_i$ - blade viscous damping coefficients $(i=1,2,\ldots,N_d)$,

$\delta$ - flap hinge axis skew angle,

$\varepsilon_{ij}$ - components of blade strain tensor $(i,j=1,2,3)$,

$\eta_i(x)$ - blade deflection modes,

$\theta_g$ - blade geometrical twist angle,

$\theta_i$ - angle of rotation in the feathering hinge of i-th blade,

$\theta_o$ - collective pitch angle,

$\lambda$ - induced velocity coefficient,

$\lambda_i$ - induced velocity perturbation coefficient,

$\lambda_o$ - constant term of induced velocity coefficient,

$\mu$ - advance ratio

$\boldsymbol{\xi}$ - section point coordinates vector, $\boldsymbol{\xi}=[0, \eta, \zeta]^T$,

$\rho$ - air density,

$\rho_b$ - blade local density,

$\tau$ - feathering axis sweep angle,

$\vartheta$ - shaft torsion angle,

$\Phi_k$ - torsion angle of the k-th blade,

$\psi$ - azimuth angle,

$\Omega$ - shaft angular velocity.

Vectors are written bold, matrices-draw.

APPENDIX 1.

Transformation matrices due to hub angles.

$$\mathbb{D} = \begin{bmatrix} \cos(\psi) & \sin(\psi) & 0 \\ -\sin(\psi) & \cos(\psi) & 0 \\ 0 & 0 & 1 \end{bmatrix}, \quad \mathbb{A}_R = \begin{bmatrix} \cos(\delta) & -\sin(\delta) & 0 \\ \sin(\delta) & \cos(\delta) & 0 \\ 0 & 0 & 1 \end{bmatrix},$$

$$\mathbb{A}_B = \begin{bmatrix} \cos(\vartheta) & \sin(\vartheta) & 0 \\ -\sin(\vartheta) & \cos(\vartheta) & 0 \\ 0 & 0 & 1 \end{bmatrix}, \quad \mathbb{B} = \begin{bmatrix} \cos(\beta) & 0 & -\sin(\beta) \\ 0 & 1 & 0 \\ \sin(\beta) & 0 & \cos(\beta) \end{bmatrix},$$

$$\mathbb{C}_1 = \begin{bmatrix} \cos(\delta) & \sin(\delta) & 0 \\ -\sin(\delta) & \cos(\delta) & 0 \\ 0 & 0 & 1 \end{bmatrix}, \quad \mathbb{C}_2 = \begin{bmatrix} \cos(\tau) & -\sin(\tau) & 0 \\ \sin(\tau) & \cos(\tau) & 0 \\ 0 & 0 & 1 \end{bmatrix},$$

$$\mathbb{G} = \begin{bmatrix} 1 & 0 & 0 \\ 0 & \cos(\theta_o) & \sin(\theta_o) \\ 0 & -\sin(\theta_o) & \cos(\theta_o) \end{bmatrix}.$$

Matrix of section rotation due to elastic deformations.

$$\mathbb{T} = \begin{bmatrix} 1 & -v'\cos(\theta_g) + w'\sin(\theta_g) & -v'\sin(\theta_g) - w'\cos(\theta_g) \\ v' & \cos(\theta_g) - \phi\sin(\theta_g) & \sin(\theta_g) + \phi\cos(\theta_g) \\ w' & -\sin(\theta_g) - \phi\cos(\theta_g) & \cos(\theta_g) - \phi\sin(\theta_g) \end{bmatrix}.$$

Vectors of translations.

$\mathbf{x}_1 = \{ x, y, z \}$, $y=\eta\cos(\theta_g)+\zeta\sin(\theta_g)$, $z=-\eta\sin(\theta_g)+\zeta\cos(\theta_g)$,

$\mathbf{s}_1 = \{-v'y, v, 0\}$, $\mathbf{s}_2=\{-w'z, 0, w\}$, $\mathbf{s}_3= \{0, -z\Phi, y\Phi\}$,

$\mathbf{x}_2 = \{x,0,0\}$, $\mathbf{v} = \{v,w,0\}$.

APPENDIX 2.

Inertia matrices.

$$B_{ni} = \int_{RA_s}\int \rho_b \left(\frac{\partial \mathbf{r}_o}{\partial q_n}\right)^T \left(\frac{\partial \mathbf{r}_o}{\partial q_1}\right) dA_s\, dR, \qquad C_{ni} = 2\int_{RA_s}\int \rho_b \left(\frac{\partial \mathbf{r}_o}{\partial q_n}\right)^T \mathbb{D}^T\dot{\mathbb{D}} \left(\frac{\partial \mathbf{r}_o}{\partial q_1}\right) dA_s\, dR,$$

$$D_{nij} = \int_{RA_s}\int \rho_b \left(\frac{\partial \mathbf{r}_o}{\partial q_n}\right)^T \left(\frac{\partial^2 \mathbf{r}_o}{\partial q_1 \partial q_j}\right) dA_s\, dR, \qquad f_1 = \int_{RA_s}\int \rho_b \left(\frac{\partial \mathbf{r}_o}{\partial q_1}\right)^T \mathbb{D}^T\ddot{\mathbb{D}}\mathbf{r}_o\, dA_s\, dR.$$

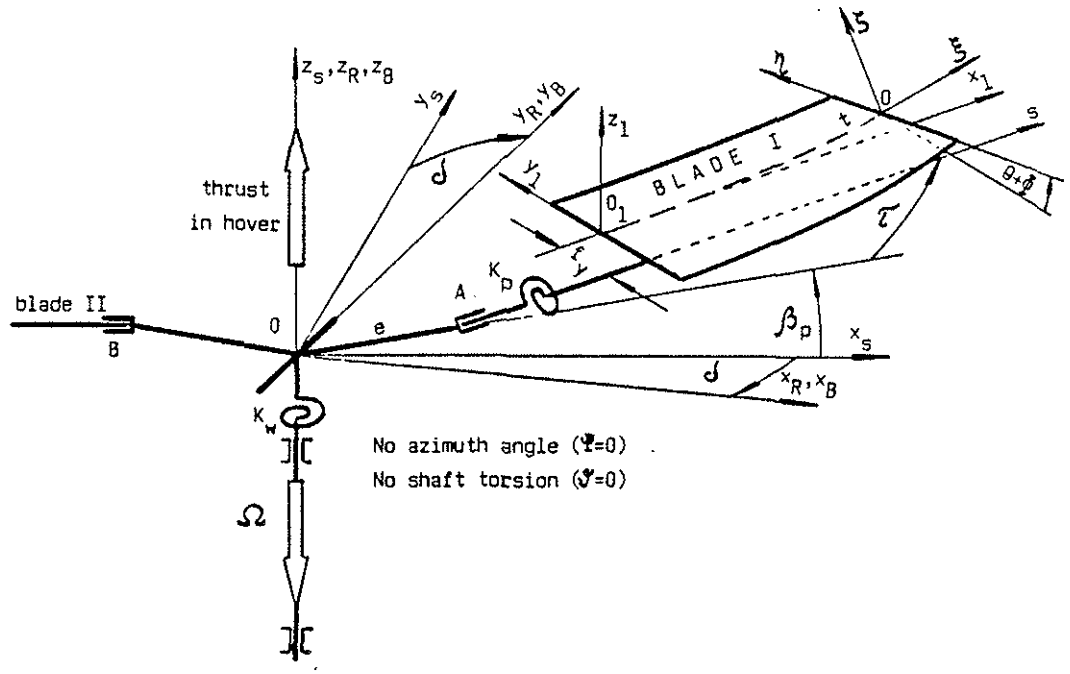


Fig.1. Model of see-saw rotor.

Table I. REAL PARTS OF EIGENVALUES

| $\mu$ | In-plane bending | | Out-of-plane bending | | Torsion | |
|---|---|---|---|---|---|---|
| | A | B | A | B | A | B |
| .0 | .469E-4 | .492E-4 | -.156E+1 | -.156E+1 | .232E-3 | .924E-4 |
| .05 | .399E-4 | .434E-4 | -.168E+1 | -.168E+1 | .571E-3 | .340E-3 |
| .10 | .522E-5 | .500E-4 | -.200E+1 | -.200E+1 | .222E-2 | .222E-2 |
| .15 | -.750E-4 | -.780E-4 | -.172E+1 | -.174E+1 | .291E-2 | .226E-2 |
| .20 | .648E-2 | .648E-2 | -.119E+1 | -.119E+1 | -.259E-3 | .511E-3 |

A - with dynamic inflow,
B - no dynamic inflow.

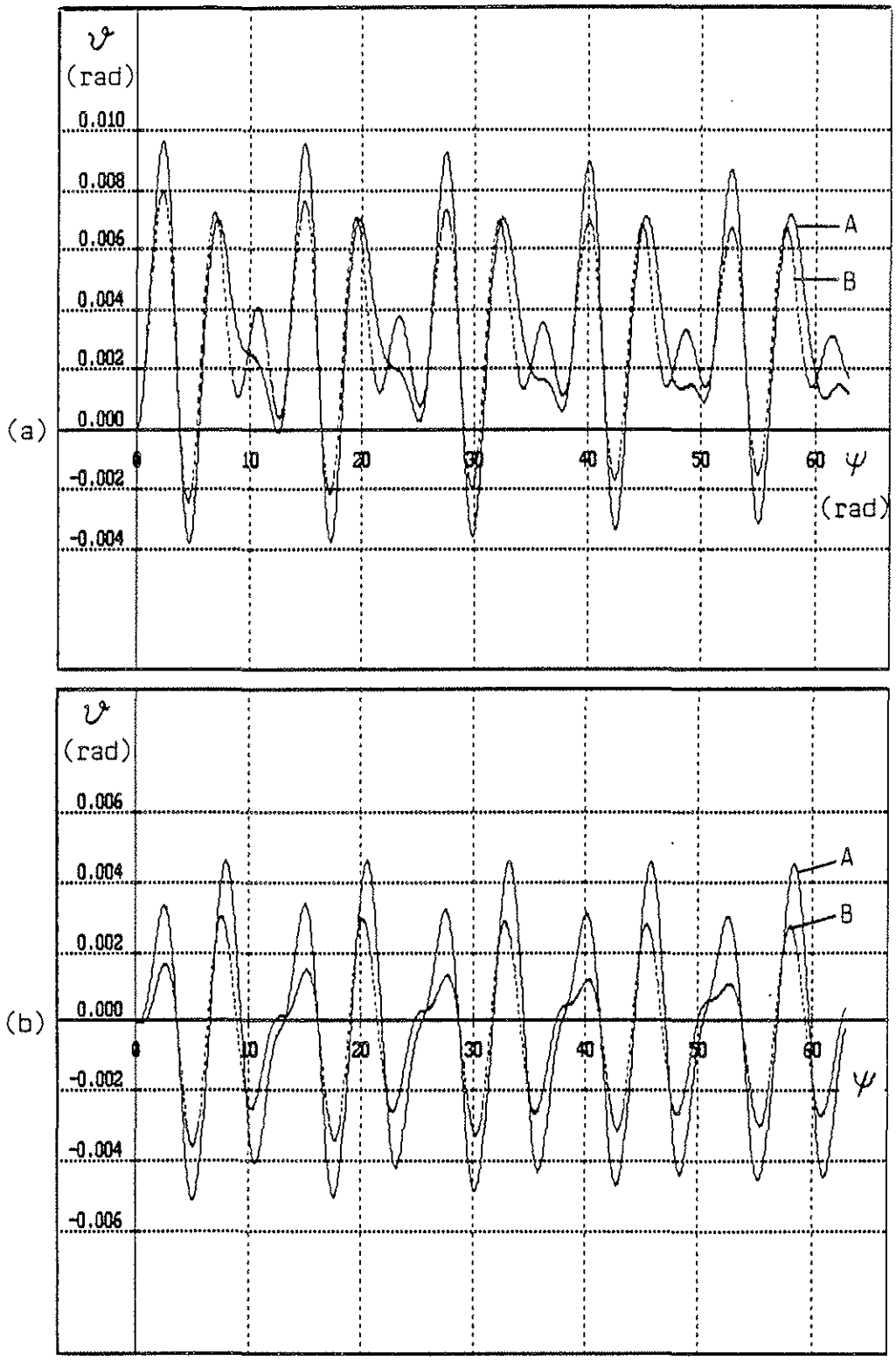


Fig.2. Shaft torsion angle vs azimuth, $\mu$ = 0.15.
(a) - with initial deflection,
(b) - no initial deflection.
A - with dynamic inflow,
B - no dynamic inflow.